HHS Public Access

Author manuscript

J Comp Neurol. Author manuscript; available in PMC 2018 December 17.

Published in final edited form as:

J Comp Neurol. 2017 June 15; 525(9): 2175–2191. doi:10.1002/cne.24196.

Comparative ultrastructural features of excitatory synapses in the visual and frontal cortices of the adult mouse and monkey

Alexander Hsu, **Jennifer I Luebke**, and **Maria Medalla**

Department of Anatomy and Neurobiology, Boston University School of Medicine, Boston, MA 02118

Abstract

The excitatory glutamatergic synapse is the principal site of communication between cortical pyramidal neurons and their targets, a key locus of action of many drugs, and highly vulnerable to dysfunction and loss in neurodegenerative disease. A detailed knowledge of the structure of these synapses in distinct cortical areas and across species is a prerequisite for understanding the anatomical underpinnings of cortical specialization and, potentially, selective vulnerability in neurological disorders. We used serial electron microscopy to assess the ultrastructural features of excitatory (asymmetric) synapses in the layers 2-3 (L2-3) neuropil of visual (V1) and frontal (FC) cortices of the adult mouse and compared findings to those in the rhesus monkey (V1 and lateral prefrontal cortex, LPFC). Analyses of multiple ultrastructural variables revealed four organizational features. First, the density of asymmetric synapses does not differ between frontal and visual cortices in either species, but is significantly higher in mouse than in monkey. Second, the structural properties of asymmetric synapses in mouse V1 and FC are nearly identical, by stark contrast to the significant differences seen between monkey V1 and LPFC. Third, while the structural features of postsynaptic entities in mouse and monkey V1 do not differ, the size of presynaptic boutons are significantly larger in monkey V1. Fourth, both presynaptic and postsynaptic entities are significantly smaller in the mouse FC than in the monkey LPFC. The diversity of synaptic ultrastructural features demonstrated here have broad implications for the nature and efficacy of glutamatergic signaling in distinct cortical areas within and across species.

Graphical Abstract Text:

Corresponding Author: Maria Medalla, Department of Anatomy and Neurobiology, Boston University School of Medicine, 72 E. Concord St. L1004, Boston, MA, 02118, USA, Tel: 617-638-5995, mmedalla@bu.edu.

Conflict of interest statement. The authors declare no conflicts of interest.

Role of authors. All authors had full access to all the data in the study and take responsibility for the integrity of the data and the accuracy of the data analysis. Study concept and design: MM, JL. Acquisition of data: AH, MM. Analysis and interpretation of data: AH, JL, MM. Drafting of the manuscript: AH, JL, MM. Critical revision of the manuscript for important intellectual content: AH, JL, MM. Statistical analysis: MM, AH. Obtained funding: MM, JL. Administrative, technical, and material support: AH, JL, MM. Study supervision: MM, JL.

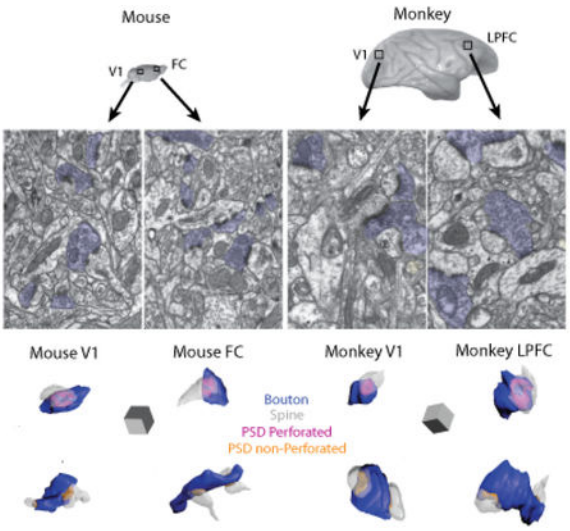

The ultrastructure of excitatory synapses in the neuropil of layers 2-3 in mouse and monkey primary visual (V1) and frontal association (mouse FC, monkey LPFC) cortices were compared using 3D serial electron microscopy. The density and location of excitatory synapses on dendritic spines versus shafts were quantified in serial EM images and reconstructed in 3D to measure the volume of presynaptic (bouton) and postsynaptic elements (postsynaptic density, PSD and spines). The authors show that the ultrastructural features of excitatory synapses of visual versus frontal cortices were markedly similar in the mouse but diverse in the monkey.

Keywords

Macaca mulatta; electron microscopy; prefrontal cortex; primary visual cortex; layers 2-3 neuropil; RRID:SCR_001914; RRID:SCR_004232; RRID:SCR_002716; RRID:SCR_002865

INTRODUCTION

Early neuroanatomists established that the mammalian cerebral cortex can be differentiated into many structurally and functionally distinct cytoarchitectonic areas (Brodmann, 1909). With the advent of high-resolution neuroimaging and neuroanatomical methods, our understanding of cortical areal heterogeneity has expanded dramatically over the past several decades. Highly detailed information about the quantitative cytoarchitecture of (i.e. cellular constituents) and connectivity between distinct cortical areas has been obtained from post-mortem histological analyses in the non-human primate animal model (Felleman and Van Essen, 1991), review: (Barbas, 2015) (Pandya et al., 2015) as well as in the human brain [review: (Zilles et al., 2004; Petrides et al., 2012). Recent studies have reliably recapitulated this detailed cortical map in the human brain using non-invasive in vivo imaging methods and novel software algorithms (Amunts and Zilles, 2015; Glasser et al., 2016). These macro-level cortical maps in humans and monkeys reflect functionally distinct cortical areas, but the detailed local circuit, cellular and subcellular underpinnings of cortical areal specialization remains to be fully elucidated. An intrinsic relationship between cortical cytoarchitecture and inter-areal connectivity is one fundamental determinant of cortical

specialization (Hilgetag et al., 2000; Hilgetag et al., 2016), review (Rakic, 2002; 2009; Barbas, 2015; Barbas and Garcia-Cabezas, 2016). The patterns of connections among distinct cortical areas are related to graded differences in cortical cytoarchitecture, such that areas with similar cytoarchitecture have the strongest inter-connections, and thus are part of the same functional network (Hilgetag et al., 2016). In line with this idea is the finding of graded differences in dendritic architecture across distinct cortical visual areas coinciding with a gradient of cortical lamination and complexity of visual information processing in the non-human primate (Elston, 2002).

That the dendritic architecture of pyramidal neurons varies depending on cortical area has been known since the time of Cajal (Ramón y Cajal, 1894; Conel, 1941; 1967; Ramón y Cajal, 1995). Recent studies have used high resolution anatomical and electrophysiological methods to further elaborate on the structural and functional properties of individual pyramidal neurons across distinct cortical areas (Elston, 2000; DeFelipe et al., 2002; Elston, 2002; 2003; Amatrudo et al., 2012; Medalla and Luebke, 2015). In the rhesus monkey, layers 2-3 (L2-3) pyramidal neurons in the LPFC and V1 are strikingly different in terms of both their morphological and electrophysiological properties. Structurally, the dendritic arbors of L2-3 pyramidal neurons in LPFC are 3-4x larger, more complex and contain ~16x higher number of dendritic spines than those of V1 (Elston, 2000; 2002; 2003; Amatrudo et al., 2012; Gilman et al., 2016). Functionally, LPFC neurons are less excitable and have significantly more frequent excitatory synaptic events with larger amplitude and longer decay time, compared to V1 neurons (Medalla and Luebke, 2015). To determine whether the differences in synaptic properties could be explained by differences in the excitatory synapses themselves, Medalla and Luebke (2015) assessed the ultrastructural properties of excitatory synapses in the layer 2/3 neuropil. Interestingly, both presynaptic boutons and postsynaptic densities of axospinous synapses were significantly larger in LPFC compared to V1. Further, there was a higher proportion of large perforated synapses in LPFC than in V1. These findings of much larger synapses in LPFC (together with the much higher density of spines) is consistent with the idea that significantly larger and more frequent synaptic currents are likely due to more numerous, larger and more powerful synapses in LPFC compared to V1.

By contrast to the highly distinctive characteristics of L2-3 pyramidal neurons in the monkey visual versus lateral prefrontal cortices, neurons in analogous areas of the mouse are remarkably similar both functionally and structurally (DeFelipe et al., 2002; DeFelipe, 2011; Gilman et al., 2016). Further, neurons in these areas differ notably between mice and monkeys (Gilman et al., 2016). For example, monkey LPFC L2-3 pyramidal neurons are significantly larger and contain more oblique dendrites than those in the mouse FC, and are also significantly less excitable with lower frequencies of excitatory synaptic events (Gilman et al., 2016). Layers 2-3 pyramidal neurons in monkey primary visual cortex also differ significantly from mouse but in different ways. Thus mouse and monkey V1 neurons are similar in size but monkey neurons have a significantly lower spine density than mouse neurons (Gilman et al., 2016). Functionally, monkey V1 neurons exhibit higher action potential firing rates and lower frequency excitatory synaptic responses than mouse V1 neurons (Gilman et al., 2016).

While these and other studies have shed light on several organizational principles of cortical parcellation, many fundamental questions about cortical anatomy at the microstructural level remain. To what extent do different cortical areas differ with regard to the nature of their cellular constituents and synaptic microcircuitry? What is the interplay between local intrinsic cellular/synaptic properties and extrinsic inputs in the mediation of functional specialization? How are unique species-specific functional capacities conferred in a given cortical area- are areas that perform putatively similar functions (e.g. first-order vision or "executive" function) organized similarly across species? Are there differences in the structural and/or functional properties of neurons and synapses in distinct cortical areas that may make them particularly susceptible to (or protected from) synaptopathy in neurodegenerative disease?

Since excitatory synaptic transmission is the fundamental driver of cortical circuit activity, a thorough knowledge of the diversity of glutamatergic synapses is a prerequisite for understanding the anatomical underpinnings of cortical specialization. It is particularly important to characterize differences that exist in these synapses between the mouse and the primate given the extensive use of mouse models in the development of human therapeutics [reviews: (Cavanaugh et al., 2014; Perrin, 2014)] as well as in large scale brain mapping projects (Egger et al., 2014; Markram et al., 2015). In order to enhance our understanding of excitatory synaptic specializations in the mouse V1 and FC compared to analogous areas in the rhesus monkey, we performed 2-D and 3-D quantitative electron microscopy analyses of asymmetric synapses in L2-3 neuropil from mouse V1 and FC and compared findings with those in the monkey.

MATERIALS AND METHODS

Experimental subjects

Brain tissue from 4 adult mice [~2 months of age, n=1 male, n=2 female; and n=1 9-14 months of age from: http://www.openconnectomeproject.org and http://dl.acm.org/citation.cfm?doid=2484838.2484870 RRID:SCR_004232 (Bock et al., 2011)] and 3 adult rhesus monkeys (ages 6-8 years old; all female) were used in this study. Some of the data on ultrastructural features of asymmetric synapses in the monkey (size of presynaptic boutons and postsynaptic spines, proportion of perforated axospinous synapses) used for comparison to mouse were previously published in Medalla and Luebke (2015). All data from mice and the following data from monkeys were generated in the current study- ultrastructural spine specializations, multisynaptic bouton features, features of asymmetric shaft synapses and relative proportions of spiny and sparsely or aspiny dendrites. Mice were housed and kept at a 12h light/dark cycle before sacrifice at Boston University School of Medicine (Boston, MA). All rhesus monkeys were part of a larger program of studies examining the impact of normal aging on the brain. Monkeys were initially obtained from the Yerkes National Primate Research Center (RRID:SCR_001914) at Emory University (Atlanta, GA). Monkeys were housed individually in the Laboratory Animal Science Center at Boston University School of Medicine and kept under a 12h light/dark cycle. The Boston University School of Medicine is fully accredited by the Association of Laboratory Animal Care with animal research and maintenance conducted in strict adherence to animal care guidelines

from the NIH Guide for the Care and use of Laboratory Animals and the U.S. Public Health Service Policy on Humane Care and Use of Laboratory Animals.

Brain tissue processing for electron microscopy (EM)

Methods used to prepare and analyze monkey V1 and LPFC tissue are described in Medalla and Luebke (2015). Mice were anesthetized with a ketamine/xylazine cocktail, and continued to be sedated with isoflurane. After a thoracotomy, animals were perfused intracardially with 1% paraformaldehyde and 1.25% glutaraldehyde in phosphate or cacodylate buffer, pH 7.4, as described previously (Ludvigson et al., 2011). Following craniotomy, the brains were removed and post-fixed in 2% PFA and 2.5% glutaraldehyde in the same buffer used for perfusion for at least 1 week at 4°C. Small 1-2 mm^3 blocks of tissue taken from the primary visual area (V1) and dorsal frontal association cortex (FC) were osmicated, dehydrated through a series of increasing ethanol concentrations (70%-100%), infiltrated with propylene oxide, and embedded in Araldite resin, as described previously (Peters et al., 2000, 2001, 2008). Tissues were counterstained either en block with 1% UA in 70% EtOH (Medalla and Barbas, 2009), or on grids (after sectioning) with 3% uranyl acetate in water and followed by 1% lead citrate (Ludvigson et al., 2011).

Sectioning and imaging for 3-Dimensional serial EM analyses

Each Araldite-embedded block was hand-trimmed to a trapezoid to include the entire depth of the cortex from the pia to the white matter and oriented so that the plane of section was parallel to the vertical axis of the apical dendrites. Semithick sections (500 nm) were cut using a diamond histo-knife (Diatome), mounted on glass slides and stained with toluidine blue for light microscopic examination and demarcation of the sampling region in L2-3. Sectioning, sampling and imaging parameters for 3D EM analyses of mouse tissue were made consistent with methods employed for monkey tissue described in Medalla and Luebke (2015). For both mouse V1 and FC, L2-3 was demarcated as beginning at ~100 μm deep to the pia and extending to ~300 μm toward the white matter. The blocks were further precision-trimmed to include the entire depth of L2-3 using a diamond trim tool (Diatome) and an ultramicrotome (Ultracut; Leica). The average block face area was about 150 × 300 μm. Approximately 40-60 serial ultrathin sections (50 nm) were then cut from each block using a diamond knife (Diatome). The ribbons of sections were collected on single slot pioloform-coated grids. Serial ultrathin sections were then examined at 80 kV using a JEOL JEM 1011 transmission electron microscope with a digital camera (Gatan). From each block, 1-2 fields devoid of cell bodies in the center of the sampling area in L2-3, approximately 200 μm deep to the pia, were photographed throughout 25-40 serial sections at 20,000X magnification. Serial images were aligned and analyzed using Reconstruct™ software (RRID:SCR_002716), as described previously (Fiala, 2005). The thickness of the imaged sections was estimated using the method of cylindrical diameters (Fiala and Harris, 2001a). The total volume analyzed per group (with an n = 3 subjects/group) was: msV1= 404 μm^3; msFC; 360 μm^3; mkV1= 1216 μm^3; mkLPFC= 1513 μm^3.

Counting and analysis of synaptic elements

Excitatory asymmetric synapses were identified based on three classic criteria: the presence of a dense postsynaptic density (PSD), round vesicles, and a wide synaptic cleft. Inhibitory

symmetric synapses were identified based on the absence of a dense PSD, pleomorphic vesicles, and a narrow synaptic cleft criteria (Peters et al., 1991). Asymmetric synapses were then further characterized based on morphology, whether they have non-perforated (continuous) PSDs versus perforated (interrupted) PSDs. Asymmetric synapses were also characterized based on features of postsynaptic targets, whether formed on spines (axospinous synapses) or on dendritic shafts (shaft synapses), and the presence of spine apparatus/smooth endoplasmic reticulum (SA/SER) in postsynaptic spine head of axospinous synapses.

Synapse densities were estimated using 3D stereologic counting methods, as described previously (Geinisman et al., 1996b; Fiala and Harris, 2001b). In all four cases, all complete synapses and incomplete synapses touching one or more inclusion borders were counted; while incomplete synapses touching any of the exclusion borders were excluded. All symmetric and asymmetric synapses completed in 3D in the series were manually traced section by section to obtain object contours of PSDs, postsynaptic spines, and presynaptic boutons. From these contours, the surface area of the PSD and the volume of spines and boutons were calculated. On average, more than ~100 synapses from 25-40 serial sections were reconstructed from each block.

We assessed the morphological features of dendrites in the volume to determine whether they are spiny dendrites, belonging to excitatory neurons, or smooth/aspiny or sparsely spiny, belonging to inhibitory neurons, according to previous criteria (Feldman and Peters, 1978; Kawaguchi et al., 2006; Medalla and Barbas, 2009). For each dendrite, we assessed qualitative features, measured the dendritic length and counted the number of shaft versus spine synapses. We calculated the density of asymmetric synapses on spines and the dendritic shaft along that length, which served as our criteria to classify dendrites. Dendrites were classified either as spiny dendrites if they had irregular undulating surfaces and had > 0.5 spine/μm and < 0.5 shaft synapse/μm, or as smooth/aspiny or sparsely spiny dendrites if they had relatively smooth surfaces and had ≤ 0.5 spine/μm and ≥ 0.5 shaft synapse/μm.

We estimated the density of spiny dendrites passing through a given volume in each tissue block. The length of each of the spiny dendrites was summed to obtain the total dendritic length in the sampled volume. The total dendritic length was then divided by the total volume of tissue sampled to estimate the density of dendrites passing per unit volume.

Statistical analyses and comparison of synaptic elements between mouse and rhesus monkey

The 3D quantitative data on synaptic features measured here in L2-3 of mouse V1 and FC were directly compared with data from monkey V1 and LPFC, newly obtained here (morphology of dendrite targets, spines with SA/SER, dendritic density) or from our previous dataset [size of presynaptic boutons and postsynaptic spines, proportion of perforated axospinous synapses; (Medalla and Luebke, 2015)]. All data were compiled in an Excel spreadsheet to calculate the mean, standard deviation and standard errors. All values were reported as mean ± SEM from multiple animals. For each variable measured, differences across the four groups (mouse V1, mouse FC, monkey V1 and monkey LPFC) were assessed using multiple comparisons ANOVA with Tukey's or Fisher's LSD post hoc

tests in SPSS (v 20, IBM Company; RRID:SCR_002865). To assess (dis)similarities across the four groups based on combination of multiple presynaptic and postsynaptic variables, multidimensional Hierarchical Clustering and Discriminant Analyses using SPSS was employed, as described (Dombrowski et al., 2001; Gilman et al., 2016). Hierarchical Clustering Analysis (HCA) was performed to determine global similarities and differences among four groups based on the multiple morphological variables measured for asymmetric axospinous synapses (a total of 10 parameters). The HCA employed squared data (dis)similarity matrices derived from pairwise comparisons of normalized morphological parameter profiles for each animal or group, which are interpreted as spatial distances and plotted as a cluster tree diagram. The distance between two branching points in a cluster tree diagram represents the relative similarity of the groups; the longer the inter-branch distance, the more dissimilar the subgroups. Discriminant Analysis (DA) was employed to assess how well each measured morphological variable segregated the individual subjects into four groups and predicted group membership. The DA identifies which experimental variables show the clearest separation of the distributions of individual subjects belonging to different groups. A discriminant score for each variable based on a discriminant function is then calculated, which is a measure of the variable's ability to predict group membership. The highest discriminant score for each function represents the best predictor of group membership. We analyzed the population distribution of asymmetric synapses for each group, calculating absolute, relative (n in each bin/total n), and cumulative frequency distribution histograms of synaptic features. A Kolmogorov-Smirnov (K-S) test was used to compare differences between population distributions. Relationships between variables were examined with linear regression analyses using Pearson's correlation.

RESULTS

Serial electron microscopy was employed to investigate the distribution and morphology of excitatory synapses in layers 2-3 (L2-3) of visual versus frontal cortices in the mouse. 3D EM data from the mouse cortices were directly compared with monkey V1 and LPFC EM data from a previous study (Medalla and Luebke, 2015) and from new analyses in the current study. Figure 1 shows visual and frontal cortices in the mouse and monkey from which blocks of tissue were obtained and prepared for EM (Fig. 1A). Semi-thin (1 μm) sections from each brain area were stained with toluidine blue to reveal neuronal somata and the surrounding neuropil in the four areas (Fig. 1B). As evident from these images, monkey LPFC has the lowest neuronal packing density among the four groups, consistent with quantitative estimates from previous studies [e.g.,(O'Kusky and Colonnier, 1982; Dombrowski et al., 2001; Hilgetag et al., 2016)].

Between-species differences in synaptic density

Asymmetric (excitatory) synapses (Fig. 1C, blue) comprised the majority of synapses in L2-3 neuropil of the four cortical areas examined (91 ± 1.9% for mouse V1; 90 ± 3.2% for mouse FC; 84 ± 4.3% for monkey V1; 88 ± 3.2% for monkey LPFC), with the remaining being symmetric (inhibitory) synapses (Fig. 2A). Within species comparisons revealed that the relative proportions of asymmetric and symmetric synapses did not differ significantly between frontal and visual cortices in both mouse and monkey (Fig. 2A). However, there

was a significant between-species difference in numerical density of asymmetric synapses, specifically the population of asymmetric synapses on dendritic spines, which was higher in both mouse V1 and FC compared to monkey V1 and LPFC ($p < 0.01$, Fig 2B, Supplemental Tables 1 and 2). Asymmetric and symmetric synapses targeted either dendritic spines (axospinous, Fig. 2F, G, I) or dendritic shafts (Fig. 2H, J).

Postsynaptic targets, location and distribution of asymmetric synapses

The majority of asymmetric synapses in all four areas (75-94%) were formed on spines and of these almost all (~99%) occurred on spine heads (Fig. 2C, F, G). Asymmetric synapses were also present on dendritic shafts (Fig 2C, D, J, K). Within species comparison showed no significant differences between V1 and FC in mouse or V1 and LPFC in monkey with regards to the density of axospinous asymmetric synapses (Fig. 2B) and the ratio of asymmetric spine:shaft synapses (Fig. 2C). The density of asymmetric shaft synapses was also similar between mouse V1 and FC, but was slightly higher in monkey V1 than in monkey LPFC ($p < 0.05$, Fig. 2B). Between-species comparisons showed that the numerical density (Fig 2B) and proportion (Fig. 2C) of asymmetric axospinous synapses were significantly higher in mouse V1 and FC compared to monkey V1 and LPFC ($p < 0.05$, Fig. 2B, C). Concomitantly, the proportion of asymmetric synapses that were on dendritic shafts was lower in mouse than in monkey cortices.

We then assessed the morphological features of dendrites targeted by shaft synapses in the four areas. We measured the length of each dendritic target and determined the density of shaft and spine asymmetric synapses along that length to classify them as either spiny dendrites (> 0.5 spine/μm, < 0.5 shaft synapse/μm) belonging to excitatory neurons, or smooth/aspiny or sparsely spiny dendrites (≤ 0.5 spine/μm and ≥ 0.5 synapse/μm) belonging to inhibitory neurons (Fig. 2D, K), consistent with previous criteria (Kawaguchi et al., 2006; Medalla and Barbas, 2009). In all four areas, the majority of shaft synapses targeted aspiny or sparsely spiny dendrites (66 ± 10% of shaft synapses in mouse V1, 77 ± 4% in mouse FC, 74 ± 10% in monkey V1, 88 ± 2% in monkey LPFC), with monkey LPFC exhibiting the highest ratio of aspiny:spiny targets. Shaft synapses targeting aspiny or sparsely spiny dendrites made up about 6 ± 3% of total asymmetric synapses in mouse V1, 4 ± 1% in mouse FC, 19 ± 6% in monkey V1 and 14 ± 2% in monkey LPFC (Fig. 2D). As with the density and proportion of total shaft asymmetric synapses, the proportion shaft asymmetric synapses specifically on aspiny or sparsely spiny dendrites, was similar between frontal and visual areas within species, but significantly higher in monkey versus mouse cortices (ANOVA, Fisher's $p < 0.05$ for all comparisons, Fig 2D). Fewer shaft synapses were formed on spiny dendrites, and these synapses made up only 3 ± 0.6% of the total asymmetric synapses in mouse V1 and 1 ±0.6% in mouse FC, 6 ± 2% in monkey V1, and 1 ± 0.4% in monkey LPFC. Multiple comparisons between and within species revealed that monkey V1 had significantly higher proportion of asymmetric shaft synapses onto spiny dendrites compared to monkey LPFC, as well as the two mouse cortices (ANOVA, Fisher's LSD, $p < 0.05$ for all comparisons, Fig 2D).

Differences in asymmetric axospinous synaptic density across the four groups can be due to differences in the density of spiny dendrites passing through the sampled volume. Thus, the

length of individual spiny dendrites, presumably belonging to excitatory neurons [(Larkman, 1991; Kawaguchi et al., 2006; Medalla and Barbas, 2009); review (Fiala et al., 2007)] was measured and summed to obtain the total dendritic length in the sampled volume. The total dendritic length was then divided by the total volume of tissue sampled to estimate the density of dendrites passing per unit volume. We then plotted asymmetric axospinous synapse density per unit volume against dendritic length per unit volume against, to roughly estimate axospinous synapses per unit length dendrite (Fig. 2E). In this plot the unitary line estimates a 1 synapse per micron dendrite length relationship. There was a trend for a lower mean dendritic length per unit volume in monkey LPFC compared to monkey V1 ($p < 0.057$). Mean dendritic length per unit volume was significantly lower in monkey LPFC than in both mouse V1 and FC cortices ($p < 0.05$), which were comparable to each other. All monkey V1 cases fall to the right of the line, indicating lower synapse per dendrite length ratio (Fig. 2E, pink). Monkey LPFC cases fall either on or to the left of the line, indicating a 1:1 or higher synapse per dendrite length ratio (Fig. 2E, red). All mouse cases fell to the left of the line, thus having a larger than 1:1 synapse per dendrite length ratio (Fig. 2E, blue).

Within-species comparison of morphological properties and size of asymmetric axospinous synapses in V1 and (LP)FC

The subset of asymmetric axospinous synapses completed serially was reconstructed in 3D together with their corresponding postsynaptic spines and presynaptic boutons when possible, in layers 2-3 neuropil of mouse V1 ($n = 178$) and mouse FC ($n = 209$) from 3 subjects, and of monkey V1 and monkey LPFC (new data and previous data from Medalla and Luebke, 2015; Figs. 3, 4, 5; Supplemental Tables 1 and 2). The synapses reconstructed in 3D were assessed for the presence of a perforation on the PSD (Fig. 3A-F), which have previously been positively correlated with receptor density and conductance [(Harris et al., 1992; Geinisman et al., 1993; Buchs and Muller, 1996; Geinisman et al., 1996a); review: (Bourne and Harris, 2008; Fukazawa and Shigemoto, 2012)]. In all four areas, the majority (65-81%) of these asymmetric synapses were simple non-perforated (Fig. 3B, C, D), and the rest were perforated (Fig, 3A, B, E; 4A). Moreover, the majority (68-85%) of spines targeted by asymmetric synapses in all areas contained a spine apparatus/smooth endoplasmic reticulum (SA/SER) in their heads (Figs. 3A-C, G; 4A), a structure associated with calcium reuptake efficacy [(Spacek and Harris, 1997; Sabatini et al., 2002); review (Nimchinsky et al., 2002; Bourne and Harris, 2008)]. In all areas, a small proportion (2-7%) of spines that received an axospinous synapse received an accompanying inhibitory synapse on either the base of its head (~68% of all symmetric axospinous synapses) or its neck (~32%; Fig. 3G).

The surface area of the PSD and volume of the targeted spine in mouse V1 and FC were largely similar, in contrast to the significant differences seen between monkey V1 and LPFC (Medalla and Luebke, 2015). Asymmetric axospinous synapses in L2-3 of monkey LPFC had more abundant perforated synapses (Fig 4A), which were associated with larger PSDs and spines (Fig. 4B, C), than in monkey V1. This regional difference in monkeys is also seen in asymmetric synapses associated with spines with SA/SER, which had larger PSD area and spine volume in LPFC than in V1 (ANOVA, Fisher's LSD post-hoc, $p < 0.05$; Fig. 4B, C). In contrast, mouse FC and V1 did not differ with respect to any of these properties. Mean overall PSD surface area and postsynaptic spine head volume of asymmetric axospinous

synapses did not differ between mouse FC and V1 (PSD area, $p = 0.52$; Spine volume, $p = 0.21$) but differed significantly between monkey LPFC and V1 ($p < 0.05$; Fig 4B, C). Multiple comparisons with data from the monkey revealed that the PSD area of asymmetric axospinous synapses in mouse FC and mouse V1 were both comparable to those in monkey V1 (monkey V1 versus mouse V1, $p = 0.87$, versus mouse FC, $p = 0.63$), but significantly smaller than those in monkey LPFC ($p < 0.05$, for all comparisons; Fig, 4B; Supplemental Table 1 and 2). Axospinous synapses in monkey LPFC had the highest proportion of perforated synapses ($p < 0.01$, Fig. 4A), and the largest PSD areas among all four groups ($p < 0.05$; Fig. 4B). A similar pattern of differences was found for spine volumes, with mouse V1 and FC showing mean spine volumes comparable to monkey V1 but significantly smaller than monkey LPFC ($p < 0.05$, Fig. 4C).

The presynaptic entity for most asymmetric synapses (87-99%) was a single bouton forming a single synapse (i.e. single-synaptic boutons). The mean volume of single-synaptic boutons did not differ in mouse V1 versus mouse FC ($p = 0.65$), but was larger in monkey LPFC than in monkey V1, specifically for those boutons associated with a perforated synapse ($p < 0.05$, Fig 5A, red asterisk). Between species comparisons showed that bouton volume in mouse FC and mouse V1 were both significantly smaller than in monkey LPFC (*$p < 0.01$) and V1 (#$p < 0.05$, Fig 5A). Axonal bouton volume of both perforated and non-perforated synapses was largest in monkey LPFC followed by monkey V1, then by mouse FC and mouse V1, which did not differ in size. There is a high degree of overlap in the mean population distribution histograms of presynaptic and postsynaptic features of asymmetric axospinous synapses between mouse V1 and FC. However, there was a modest difference in the population distribution based on PSD area and postsynaptic spine volume (K-S test, $p < 0.01$), but not presynaptic bouton volume (Fig. 5B). Specifically, cumulative frequency distributions of mouse V1 synapses were shifted to the right, indicating a slightly higher frequency of synapses with large PSD and spines, compared to mouse FC. Our previous data in monkey showed the opposite trend; monkey V1 synapse population distribution had a higher frequency of small synapses and spines compared to monkey LPFC (Medalla and Luebke, 2015).

A small proportion of boutons formed synapses with two or more postsynaptic sites (multi-synaptic boutons; MSBs). MSBs were more prevalent in mouse cortex then in monkey ($p < 0.05$; Supplemental Tables 1 and 2), comprising 10-17% of the total excitatory boutons in mouse V1; 5-15% in mouse FC; 2.7-3.7% in monkey V1 and 1.3-5% for monkey LPFC. These proportions were consistent with previous 3D EM studies, which quantified the frequency of MSBs in layer 2-3 neuropil of mouse [~18% of excitatory boutons in mouse somatosensory cortex; (Kasthuri et al., 2015)] and monkey cortices [~6% of excitatory boutons in monkey LPFC; (Medalla and Barbas, 2009)].

Within-species comparisons showed that the proportion of MSBs forming asymmetric synapses on more than one spine/dendrite did not differ significantly between frontal and visual cortices in either mouse and monkey. The majority (75-90%) of MSB synapses were associated with non-perforated PSDs. Consistent with the single-synaptic boutons, the mean volumes of MSBs in both mouse V1 and FC (n = 16 MSBs reconstructed from each area) were significantly smaller than in monkey V1 and LPFC (n=7 MSBs reconstructed from

each area; $p < 0.05$), with no marked within-species differences ($p=0.39$ for mouse; $p=0.86$ for monkey; Fig. 5A).

Positive Linear Relationship between Presynaptic and Postsynaptic Entities

Relationships between 3D reconstructed presynaptic and postsynaptic entities of L2-3 neuropil of mouse FC and V1 (Fig. 5D) were assessed and compared with monkey V1 and LPFC using linear regression analysis (Fig. 5C). Linear regression analysis showed a strong positive correlation of PSD area with the volume of the postsynaptic spine was found among mouse V1 ($r = 0.84$), mouse FC ($r = 0.9$), monkey V1 ($r = 0.73$) and monkey LPFC ($r = 0.87$, $p < 0.001$; Fig. 5C). For boutons forming single synapses, the PSD area was also correlated with the volume of presynaptic bouton, a relationship stronger in mouse V1 ($r = 0.75$), mouse FC ($r = 0.85$) and monkey LPFC ($r = 0.81$), than in monkey V1 ($r = 0.3$, $p < 0.001$; Fig. 5C). The linear relationship between synapse size and the size of presynaptic and postsynaptic elements in V1 and (LP)FC in both mouse and monkey is consistent with the findings in other areas of the rodent cortex [e.g., (Harris et al., 1992; Rollenhagen et al., 2015); for review, see (Rollenhagen and Lubke, 2006; Bourne and Harris, 2008)], and in many areas of the monkey [e.g., (Germuska et al., 2006; Medalla et al., 2007; Zikopoulos and Barbas, 2007; Medalla and Barbas, 2010; Timbie and Barbas, 2014)].

There were no significant correlations between MSB volume and size of the individual synapses they formed or with postsynaptic spine volume. However, there was a positive linear correlation between MSB volume and the summed areas of their PSDs in mouse V1 ($r =0.83$), mouse FC ($r = 0.87$), and monkey V1 ($r = 0.95$; $p < 0.05$), but not in monkey LPFC ($r = 0.17$) (Fig. 5F). Typically, MSBs formed synapses on two (more rarely on three) postsynaptic spines (Fig. 5E), as has previously been reported (Bartol et al., 2015; Kasthuri et al., 2015). Here, we observed that spines innervated by the same MSB often differed in size in all areas and that there was a positive correlation between the volume of the “larger” spine and that of the “smaller” spine for the population of MSBs examined for the monkey LPFC only ($r = 0.92$; $p < 0.05$) (Fig. 5F).

Degree of similarity between visual and frontal cortices in mouse versus monkey based on multiple excitatory synaptic features

To assess the relative similarities of the four areas (mouse V1, mouse FC, monkey V1, and monkey LPFC) and how well these areas segregated based on the combination the multiple variables measured to characterized asymmetric axospinous synapses, we used discriminant and hierarchical clustering analyses based on these 10 parameters: asymmetric synaptic density, PSD area, spine volume and presynaptic bouton volume of perforated and non-perforated synapses, PSD area and spine volume of synapses onto spines with SA/SER, proportion of perforated synapses.

To assess the (dis)similarities across the 12 distinct tissue blocks from 4 individual subjects and across the four groups overall (mouse FC, mouse V1, monkey LPFC, and monkey V1), when all 9 variables of asymmetric axospinous synapses were considered in concert in a multidimensional scale, Hierarchical Clustering Analysis (HCA) was performed (Fig. 6A, B). Hierarchical clustering based on parameters from each individual animal (Fig 6A) and

from the mean of each group (Fig. 6B) revealed that monkey LPFC is the most different group, and that monkey V1 and LPFC are more dissimilar from each other than mouse V1 and FC. Dendrogram plots based on squared Euclidean distances showed that, all the three individual monkey LPFC cases clustered together and branched off earliest and had the largest Euclidean and branching distance (the most dissimilar) from the other groups (Fig. 6A). Dendrograms also showed that, with the exception of one mouse FC and V1 case, mouse V1 and FC were more similar to each other, having an inter-branch distance smaller than between than monkey LPFC and V1. In contrast, monkey V1 and monkey LPFC cases each formed distinct clusters, which had large inter-branch distances, and are therefore more dissimilar from each other compared to mouse V1 and FC. Consistent with HCA of individual cases, HCA based on all mean asymmetric axospinous synaptic properties of each group showed that monkey V1 versus monkey LPFC segregated from each other to a greater degree than mouse V1 and mouse FC (Fig. 6B).

Discriminant analysis (DA) was employed to assess how well the set of asymmetric axospinous synaptic variables segregated each case into the four groups and predicted group membership (Fig. 6C). For the set of variables characterizing asymmetric axospinous synapses, DA separated the data into four groups, with the most significant and strongest segregation between monkey LPFC and the rest of the groups (Fig. 6C). Among the variables, volume of spines associated with perforated synapses and SA/SER had the highest discriminant scores, and therefore the most the reliable discriminators of group membership. Consistent with multiple comparison ANOVA analyses and the HCA, a scatter plot based on these discriminant functions derived from features of asymmetric axospinous synapses showed more segregation of data points between monkey V1 and LPFC than between mouse V1 and FC, suggesting a more homogenous L2-3 neuropil in mouse than in cortical areas between mouse and monkey.

DISCUSSION

In the ongoing effort to gain a detailed understanding of the microcircuitry of diverse cortical areas across species we performed a comprehensive assessment of excitatory synapses in the L2-3 neuropil of the mouse V1 and FC and compared findings to those from functionally analogous areas in the rhesus monkey [some of which was previously published in (Medalla and Luebke, 2015)]. Consistent with our previous work demonstrating the similarity of L3 neurons in mouse V1 and FC (Gilman et al., 2016), we found that excitatory synapses are also virtually identical, with regard to: density, location, size of pre- and post-synaptic elements and prevalence of both perforated synapses and spines containing SA/SER. By contrast, excitatory synapses in monkey V1 and LPFC differ dramatically- with a much higher prevalence of large perforated synapses in LPFC concomitant with significantly larger spines and presynaptic boutons (Medalla and Luebke, 2015). With regard to species comparisons, there is a higher density of excitatory synapses in both mouse areas compared to monkey. While the structural features of postsynaptic entities in mouse and monkey V1 do not differ, the size of presynaptic boutons is significantly larger in monkey V1. Finally, both presynaptic and postsynaptic entities are significantly smaller in the mouse FC than in the monkey LPFC. The overarching significance of the work is that the ultrastructural features of excitatory symmetric synapses are nearly identical in mouse V1 and FC, while

they differ significantly in the monkey V1 and LPFC. These findings are consistent with our previous work showing that the morphological and physiological properties of L3 pyramidal neurons mouse neocortical areas V1 and FC are nearly identical while these neurons in the monkey V1 and LPFC are markedly different.

Species differences in excitatory synapse density and location

In our previous study using 3D high-resolution confocal imaging of biocytin-filled L3 pyramidal neurons we reported that mouse FC, mouse V1 and monkey LPFC neurons do not differ with regard to spine density and that each has a significantly higher spine density than do those in monkey V1 (Gilman et al., 2016). All else being equal, these data would have predicted approximately equivalent synapse density in mouse FC, V1 and monkey LPFC and lower densities in monkey V1. On the contrary, here we observe a higher density of asymmetric axospinous synapses in FC and V1 in mouse compared to *both* monkey V1 *and* LPFC, where synapse density is equivalent. What might account for the apparent discrepancy in confocal (spine) and electron microscopic (synapse) findings? Perhaps the most straightforward explanation is a significantly lower density of neurons in monkey LPFC than in monkey V1 and in mouse V1 and FC. To elaborate, compared to mouse V1 and FC, [which each contain ~9.2×10^4 neurons/mm^3;(Schuz and Palm, 1989)] and to monkey V1 [which contains ~11.9×10^4 neurons/mm^3; (O'Kusky and Colonnier, 1982)], monkey LPFC contains larger neurons that are less densely packed, [~4.0×10^4 neurons/mm^3; (Dombrowski et al., 2001)]. Since monkey V1 has more neurons than monkey LPFC, but axospinous synaptic density is similar between monkey V1 and LPFC (Medalla and Luebke, 2015), it follows that the number of synapses per neuron is lower in V1 versus LPFC. This is consistent with the fact that both density and number of spines on individual L3 neurons are lower in V1 neurons than in LPFC (Amatrudo et al., 2012; Medalla and Luebke, 2015). Indeed here we show that there is higher dendritic packing density per unit volume in V1 than in LPFC. With axospinous synapse density being equal in the two regions, we show a lower axospinous synapse per dendritic length ratio in a given volume in monkey V1 than in monkey LPFC. This synapse:dendritic length ratio provides a rough estimate of the average spine density in each area, which is lower in V1 than in LPFC, again consistent with the difference in the density of spines on individual L3 neurons from the two areas that we have previously reported (Amatrudo et al., 2012; Medalla and Luebke, 2015).

We cannot rule out that another plausible contributor to the difference in confocal (spine) versus EM (synapse) density findings is the difference in sampling locus between the two methods. Confocal data was obtained from individual L3 neurons in which spines were counted across the entirety of the filled dendritic arbor, while the EM-sampled volume is comprised of a mixed population of dendrites from many different neurons (and neuron types). Thus, using standard EM methodology we are unable to distinguish axospinous synapses impinging on dendrites from L3 pyramidal neurons, from those that impinge upon distal dendrites of L5-6 pyramidal neurons or upon sparsely spiny interneurons [e.g., (Feldman and Peters, 1978; Peters and Sethares, 1991) (Kawaguchi et al., 2006)]. It is possible that the proportions of dendrites from distinct neuronal populations passing through L2-3 differ between mouse and monkey cortical areas, resulting in distinct spine and synapse densities in different regions. Indeed our findings and those of others are consistent

with this idea, in that there is a significantly higher proportion of shaft synapses in L2-3 neuropil of monkey LPFC and V1 than in mouse FC and V1. The majority of the shaft synapses quantified here, especially in monkey LPFC, are located on aspiny or sparsely spinous dendrites, which are characteristic of inhibitory interneurons [(Feldman and Peters, 1978; Kawaguchi et al., 2006; Medalla and Barbas, 2009; 2010); review (Fiala et al., 2007)]. In addition, compared to mouse cortices and to monkey LPFC, monkey V1 also has a relatively higher proportion of synapses innervating shafts of spiny dendrites, with low shaft synapse density per length. These data suggest that the proportion of aspiny, sparsely spiny and spiny dendrites from inhibitory and excitatory neurons in L2-3 likely differ between monkey V1 and monkey LPFC, and between monkey and mouse. Moreover, previous large-scale 3D EM studies in mouse V1 suggest that sources of asymmetric synapses on shafts of inhibitory neurons also differ between mouse and monkey (Bopp et al., 2014). In mouse V1, up to ~50% of asymmetric synapses from local axon collaterals of individual L2-3 pyramidal neurons preferentially target shafts of smooth dendrites of inhibitory neurons (Bock et al., 2011; Bopp et al., 2014), a proportion that is significantly higher than in monkey LPFC and V1 (McGuire et al., 1991; Melchitzky et al., 1998). Thus, given the higher overall proportion of asymmetric shaft synapses in monkey versus mouse, these data suggest that in the monkey there is a smaller contribution of local axon collaterals and a larger contribution of extrinsic synapses from other brain areas to the innervation of inhibitory neurons [see also (Medalla and Barbas, 2009; Bopp et al., 2014)]. Further work on 3D EM assessments of immunohistochemically-labeled populations of inhibitory neurons and pathways [e.g., (Medalla and Barbas, 2009)] or using large-scale volumetric EM methods [e.g., (Bartol et al., 2015; Kasthuri et al., 2015)] are needed to characterize sources of synapses impinging on specific neuronal populations and somatodendritic loci in the two cortical areas in mouse and monkey.

Within-species comparison of excitatory synapse ultrastructure in functionally distinct cortical areas

The ultrastructural features of excitatory synapses in L2-3 of mouse V1 and FC are identical with regard to presynaptic bouton and postsynaptic spine head volumes, PSD surface area, proportion of perforated PSDs and proportion of spine heads containing a SA/SER. These findings are in marked contrast to the significant differences in the sizes of these pre- and post-synaptic entities and the proportion of perforated PSDs in monkey V1 versus LPFC (Medalla and Luebke, 2015). Consistent with this demonstration of the structural similarity of excitatory synapses in mouse V1 and FC, we have previously reported that excitatory postsynaptic currents in L3 pyramidal neurons in these two areas of the mouse brain are the same with regard to frequency, amplitude and kinetics (Gilman et al., 2016), whereas they differ markedly in the monkey (Amatrudo et al., 2012; Medalla and Luebke, 2015). This consistency in structural and functional data is not surprising in light of studies demonstrating correlations between ultrastructural features and synaptic response properties. Specifically, the volume of boutons, the volume of spine heads, the proportion and volume of spines containing SA/SER, and the proportion and surface area of perforated PSD are some of the many interacting structural variables that determine synaptic efficacy (Tong and Jahr, 1994; Baude et al., 1995; Murthy et al., 1997; Nusser et al., 1998; Takumi et al., 1999;

Matsuzaki et al., 2001; Murthy et al., 2001; Schikorski and Stevens, 2001; Li et al., 2005; Germuska et al., 2006; Zikopoulos and Barbas, 2007).

Between-species comparison of excitatory synapse ultrastructure in visual and frontal cortices

Direct comparison of excitatory synapses in L2-3 neuropil of analogous frontal and visual cortical areas in mouse versus monkey revealed marked differences in presynaptic and postsynaptic structures between species. The L2-3 neuropil of monkey LPFC contained a significantly higher number of perforated PSDs and larger spine volume at perforated synapses as well as larger spine volumes of SA/SER-containing spines compared to L2-3 neuropil of mouse FC. Since both synapse size and proportion of perforated excitatory synapses were all larger in monkey than in mouse frontal cortex, it would be expected (all other things being equal) that synaptic responses would be higher in amplitude (and possibly frequency) in monkey neurons, yet this is not the case. Instead, the spontaneous excitatory postsynaptic current (sEPSC) responses of monkey LPFC neurons do not differ from mouse FC neurons with regard to amplitude or kinetics (Gilman et al., 2016), but are lower in frequency. It is possible that this unexpected relationship can be accounted for by greater levels of dendritic filtering and thus a greater degree of attenuation of EPSCs across the much longer dendritic arbors of monkey LPFC neurons (Rall, 1962; 1964; Elston, 2002; Amatrudo et al., 2012; Medalla and Luebke, 2015); reviewed in (London and Hausser, 2005; Spruston, 2008)]. Moreover, the higher frequency of MSBs in mouse FC compared to monkey LPFC can also strengthen synaptic responses when targeting spines emanating from the same parent dendrite (Bartol et al., 2015), by virtue of a higher probability of neurotransmitter release from multiple synaptic sites that can lead to increased EPSC amplitude and frequency [e.g., (Murthy et al., 1997; Raghavachari and Lisman, 2004)]. Future studies will be required to untangle the many factors that determine the synaptic filtering and processing through the complex dendritic arbors and the release properties and efficacy of MSBs in each of these areas.

By contrast to the axospinous synapses in frontal cortices, those in the L2-3 neuropil of monkey and mouse V1 differed only in size of presynaptic entities (being significantly larger in monkey), with postsynaptic entities being the same. Interestingly, monkey V1 neurons exhibit sEPSCs with significantly lower frequency, smaller amplitude and shorter decay time than mouse V1 neurons (Gilman et al., 2016). Although there were relatively more large boutons in L2-3 neuropil of monkey V1 compared to that of mouse V1, the monkey V1 boutons analyzed had a weak correlation with vesicle number ($r = 0.3$), consistent with the finding that there are large boutons in monkey V1 with few synaptic vesicles. In addition, mouse V1 neurons have a significantly higher spine density than do monkey V1 neurons, which also likely contributes to both the higher amplitude and higher frequency of EPSCs observed in mouse compared to monkey V1 L3 pyramidal neurons.

Our findings show that there are species-specific differences in the relationships between the size of pre- and post-synaptic elements. For both mouse V1 and FC, bouton volume correlated with total PSD area for both single and multi-synaptic boutons. However in monkey, the volume of single synaptic boutons did not correlate with PSD area in monkey

V1, and the volume of MSBs did not correlate with total PSD area in monkey LPFC. The strength and nature of the correlation between pre- and post-synaptic structural size is related to the extent of synapse rewiring and stability [e.g., (Meyer et al., 2014); reviewed in (Holtmaat and Svoboda, 2009; Harris and Weinberg, 2012)]. The species-specific relationships of bouton volume and PSD area examined here suggest that monkey and mouse cortices have distinct rules for synaptic plasticity. Consistent with this idea, our findings and previous work in other mouse cortical areas (Kasthuri et al., 2015) show that both mouse V1 and FC have a higher proportion of multisynaptic boutons forming asymmetric synapses on two or more spines, compared to monkey V1 and LPFC. On the other hand, monkey LPFC has a higher proportion of perforated synapses compared to mouse cortex. These data suggest that while MSB formation is a prominent form of plasticity in mouse cortices, the formation of perforated PSDs is a uniquely predominant manifestation of synaptic plasticity in monkey LPFC [reviewed in (Harris and Weinberg, 2012)].

Comparison to previous studies

Previous studies have estimated the density and proportion of the postsynaptic components of excitatory synapses in L2-3 of mouse and monkey visual and frontal cortices using 2D EM methods (Schuz and Palm, 1989; Peters et al., 2008; Crimins et al., 2011; Luebke et al., 2013). The proportions of postsynaptic targets and synapse morphological types based on these 2D methods are highly consistent with the 3D data in the current study, but there is some variability in the estimates of numerical synapse density likely due to differences in methodological counting and sampling parameters, processing methods and subjects. Some tissue blocks analyzed in previous 2D EM work in monkey V1 and LPFC from our group (Peters et al., 2008; Luebke et al., 2013) were obtained from the same animals that were used for the current 3D EM study. Direct comparisons of 2D and 3D methods in these animals reveal that even if there were small differences in 2D versus 3D absolute synapse density estimates, the relative differences across animals and areas were consistent between the two methods. While there have been few 3D EM studies of excitatory synapses in the rhesus monkey cortex [but see (Medalla et al., 2007; Medalla and Barbas, 2009; 2010)], comparatively extensive 3D EM work has been done in L2-3 of mouse primary visual cortex-comparing synapses from identified neurons (Bock et al., 2011) and the general population of excitatory synapses in L2-3 neuropil (Bopp et al., 2014). Data on numerical densities and proportion of axospinous and shaft synapses from these studies are consistent with the present findings. Further, 3D measurements of synapse size from the present study (PSD area, spine volume, and bouton volume) have means and range of values comparable to data from previous large-scale 3D EM studies in mouse [e.g.,(Harris and Weinberg, 2012; Kasthuri et al., 2015)] and monkey cortices [e.g.,(Medalla and Barbas, 2010; Timbie and Barbas, 2014)]. Although the current study has a relatively limited z-sampling per sample site compared to previous large-scale EM studies, the increased sampling across different areas and animals allowed direct comparisons between frontal and visual areas in mouse versus monkey cortex using 3D EM for the first time.

Implications of findings

The present study demonstrates that mouse V1 and mouse FC are virtually identical in terms of the presynaptic and postsynaptic ultrastructural features of excitatory synapses in L2-3 neuropil. Unlike in the mouse, there are marked differences in the size, structure and physiology of individual L3 pyramidal neurons, and in presynaptic and postsynaptic ultrastructural features of excitatory synapses in area V1 compared to area LPFC in the rhesus monkey (Amatrudo et al., 2012; Medalla and Luebke, 2015). In a previous study, we also demonstrated that mouse V1 resembles mouse FC at the single cell level, with individual L3 pyramidal neurons having similar size, dendritic extent and topology, as well as in intrinsic membrane, action potential firing and synaptic response properties (Gilman et al., 2016).

Taken together, data from this and previous studies predict that, in mice, excitatory synaptic transmission at the cellular and local circuit levels in L2-3 of V1 and FC is very similar –if not identical- both structurally and functionally. In this species, both the unimodal primary sensory area V1 and multimodal FC contain cellular and synaptic features consistent with a relatively highly excitable circuit, being comprised of small and electrically compact output neurons, and abundant asymmetric axospinous synapses on each pyramidal neuron. Moreover, our data suggest that the capacity and mechanisms for synaptic plasticity, based on the frequency of MSBs and the size relationship of pre- and post-synaptic entities, is similar between mouse V1 and FC areas. This is interesting in light of the body of work showing synaptic plasticity *in vivo* in mouse V1 beyond the classic “critical period” [reviewed in (Tropea et al., 2009)]. Based on data presented here, the mechanisms of synaptic plasticity observed from these studies in mouse V1 may similarly apply to mouse FC [e.g., (Gavornik and Bear, 2014)]. However, the synaptic features of mouse frontal and visual areas are distinct from the analogous monkey visual and frontal areas, and thus, mechanisms for plasticity likely differ between these species [e.g., (Verhoog et al., 2013; Testa-Silva et al., 2014; Nys et al., 2015)].

In contrast to mouse cortices, excitatory synaptic transmission differs markedly in monkey V1 and LPFC, with cellular and synaptic features indicative of distinct cellular excitability, as well as distinct dynamic range and temporal scale of synaptic transmission. The sparsely connected and electrically compact L3 pyramidal neurons in monkey V1 form circuits that are well suited for rapid synaptic transmission with a relatively high degree of input-output fidelity [for review, see (Olshausen and Field, 2004; Vogels et al., 2005; Panzeri et al., 2010)]. On the other hand, the multimodal association LPFC in monkey is comprised of cellular and synaptic features consistent with more powerful and longer-lasting inputs, and having large and electrotonically complex L3 output neurons. These features facilitate sustained activation, coincidence detection, and spike-timing-dependent plasticity that are optimal for integrative functions such as decision making and sensorimotor interactions [for review, see (Constantinidis and Wang, 2004; Sjostrom et al., 2008)].

In conclusion, our data provide further evidence that frontal and visual areas are relatively homogenous in mouse but markedly different in the monkey. These data are important for understanding how excitatory signaling within neuronal networks differs between rodents

and primates (DeFelipe et al., 2002) and of how cortical microcircuitry contributes to the unique functions of diverse cortical areas in distinct animal models.

Supplementary Material

Refer to Web version on PubMed Central for supplementary material.

Acknowledgments

Support: This work was supported by NIH/NIA grants P01-AG00001, R01 AG025062, R01 AG035071 and NIH/MH grant K99 and R00 MH101234.

Other acknowledgments. We are grateful to Drs. Davi Bock and Clay Reid and to the Connectome Project: http://www.openconnectomeproject.org, for providing public access to an EM volume of mouse area V1. Ultrastructural properties of synapses in layer 2-3 neuropil for one mouse area V1 were assessed from these data, which are available in the http://openconnecto.me/bock11/ database originally published as doi:10.1038/nature09802 and at http://dl.acm.org/citation.cfm?doid=2484838.2484870.

REFERENCES

Amatrudo JM, Weaver CM, Crimins JL, Hof PR, Rosene DL, Luebke JI. 2012 Influence of highly distinctive structural properties on the excitability of pyramidal neurons in monkey visual and prefrontal cortices. J Neurosci 32(40):13644–13660. [PubMed: 23035077]

Amunts K, Zilles K. 2015 Architectonic Mapping of the Human Brain beyond Brodmann. Neuron 88(6):1086–1107. [PubMed: 26687219]

Barbas H 2015 General cortical and special prefrontal connections: principles from structure to function. Annual review of neuroscience 38:269–289.

Barbas H, Garcia-Cabezas MA. 2016 How the prefrontal executive got its stripes. Curr Opin Neurobiol 40:125–134. [PubMed: 27479655]

Bartol TM, Bromer C, Kinney J, Chirillo MA, Bourne JN, Harris KM, Sejnowski TJ. 2015 Nanoconnectomic upper bound on the variability of synaptic plasticity. eLife 4:e10778. [PubMed: 26618907]

Baude A, Nusser Z, Molnar E, McIlhinney RA, Somogyi P. 1995 High-resolution immunogold localization of AMPA type glutamate receptor subunits at synaptic and non-synaptic sites in rat hippocampus. Neuroscience 69(4):1031–1055. [PubMed: 8848093]

Bock DD, Lee WC, Kerlin AM, Andermann ML, Hood G, Wetzel AW, Yurgenson S, Soucy ER, Kim HS, Reid RC. 2011 Network anatomy and in vivo physiology of visual cortical neurons. Nature 471(7337):177–182. [PubMed: 21390124]

Bopp R, Macarico da Costa N, Kampa BM, Martin KA, Roth MM. 2014 Pyramidal cells make specific connections onto smooth (GABAergic) neurons in mouse visual cortex. PLoS Biol 12(8):e1001932. [PubMed: 25137065]

Bourne JN, Harris KM. 2008 Balancing structure and function at hippocampal dendritic spines. Annual review of neuroscience 31:47–67.

Buchs PA, Muller D. 1996 Induction of long-term potentiation is associated with major ultrastructural changes of activated synapses. Proc Natl Acad Sci U S A 93(15):8040–8045. [PubMed: 8755599]

Cavanaugh SE, Pippin JJ, Barnard ND. 2014 Animal models of Alzheimer disease: historical pitfalls and a path forward. ALTEX 31(3):279–302. [PubMed: 24793844]

Conel JL. 1941 The cortex of a one month old infant. Conel JL, ed. Cambridge, MA: Harvard University Press.

Conel JL. 1967 The cortex of a six year old child. Conel JL, ed. Cambridge, MA: Harvard University Press.

Constantinidis C, Wang XJ. 2004 A neural circuit basis for spatial working memory. The Neuroscientist : a review journal bringing neurobiology, neurology and psychiatry 10(6):553–565.

Crimins JL, Rocher AB, Peters A, Shultz P, Lewis J, Luebke JI. 2011 Homeostatic responses by surviving cortical pyramidal cells in neurodegenerative tauopathy. Acta neuropathologica 122(5): 551–564. [PubMed: 21968531]

DeFelipe J 2011 The evolution of the brain, the human nature of cortical circuits, and intellectual creativity. Front Neuroanat 5:29. [PubMed: 21647212]

DeFelipe J, Alonso-Nanclares L, Arellano JI. 2002 Microstructure of the neocortex: comparative aspects. Journal of neurocytology 31(3-5):299–316. [PubMed: 12815249]

Dombrowski SM, Hilgetag CC, Barbas H. 2001 Quantitative architecture distinguishes prefrontal cortical systems in the rhesus monkey. Cereb Cortex 11(10):975–988. [PubMed: 11549620]

Egger R, Dercksen VJ, Udvary D, Hege HC, Oberlaender M. 2014 Generation of dense statistical connectomes from sparse morphological data. Front Neuroanat 8:129. [PubMed: 25426033]

Elston GN. 2000 Pyramidal cells of the frontal lobe: all the more spinous to think with. J Neurosci 20(18):RC95. [PubMed: 10974092]

Elston GN. 2002 Cortical heterogeneity: implications for visual processing and polysensory integration. Journal of neurocytology 31(3-5):317–335. [PubMed: 12815250]

Elston GN. 2003 Cortex, cognition and the cell: new insights into the pyramidal neuron and prefrontal function. Cereb Cortex 13(11):1124–1138. [PubMed: 14576205]

Feldman ML, Peters A. 1978 The forms of non-pyramidal neurons in the visual cortex of the rat. J Comp Neurol 179(4):761–793. [PubMed: 346619]

Felleman DJ, Van Essen DC. 1991 Distributed hierarchical processing in the primate cerebral cortex. Cereb Cortex 1(1):1–47. [PubMed: 1822724]

Fiala J, Spacek J, Harris KM. 2007 Dendrite structure In: Stuart G, Spruston N, Hausser M, eds. Dendrites. 2 ed. New York, NY: Oxford University Press.

Fiala JC. 2005 Reconstruct: a free editor for serial section microscopy. Journal of microscopy 218(Pt 1):52–61. [PubMed: 15817063]

Fiala JC, Harris KM. 2001a Cylindrical diameters method for calibrating section thickness in serial electron microscopy. Journal of microscopy 202(Pt 3):468–472. [PubMed: 11422668]

Fiala JC, Harris KM. 2001b Extending unbiased stereology of brain ultrastructure to three-dimensional volumes. Journal of the American Medical Informatics Association : JAMIA 8(1):1–16. [PubMed: 11141509]

Fukazawa Y, Shigemoto R. 2012 Intra-synapse-type and inter-synapse-type relationships between synaptic size and AMPAR expression. Curr Opin Neurobiol 22(3):446–452. [PubMed: 22325858]

Gavornik JP, Bear MF. 2014 Higher brain functions served by the lowly rodent primary visual cortex. Learn Mem 21(10):527–533. [PubMed: 25225298]

Geinisman Y, deToledo-Morrell L, Morrell F, Heller RE, Rossi M, Parshall RF. 1993 Structural synaptic correlate of long-term potentiation: formation of axospinous synapses with multiple, completely partitioned transmission zones. Hippocampus 3(4):435–445. [PubMed: 8269035]

Geinisman Y, Detoledo-Morrell L, Morrell F, Persina IS, Beatty MA. 1996a Synapse restructuring associated with the maintenance phase of hippocampal long-term potentiation. J Comp Neurol 368(3):413–423. [PubMed: 8725348]

Geinisman Y, Gundersen HJ, van der Zee E, West MJ. 1996b Unbiased stereological estimation of the total number of synapses in a brain region. Journal of neurocytology 25(12):805–819. [PubMed: 9023726]

Germuska M, Saha S, Fiala J, Barbas H. 2006 Synaptic distinction of laminar-specific prefrontal-temporal pathways in primates. Cereb Cortex 16(6):865–875. [PubMed: 16151179]

Gilman JP, Medalla M, Luebke JI. 2016 Area-Specific Features of Pyramidal Neurons-a Comparative Study in Mouse and Rhesus Monkey. Cereb Cortex. 2016 3 10. pii: bhw062. [Epub ahead of print].

Glasser MF, Coalson TS, Robinson EC, Hacker CD, Harwell J, Yacoub E, Ugurbil K, Andersson J, Beckmann CF, Jenkinson M, Smith SM, Van Essen DC. 2016 A multi-modal parcellation of human cerebral cortex. Nature 536(7615):171–178. [PubMed: 27437579]

Harris KM, Jensen FE, Tsao B. 1992 Three-dimensional structure of dendritic spines and synapses in rat hippocampus (CA1) at postnatal day 15 and adult ages: implications for the maturation of synaptic physiology and long-term potentiation. J Neurosci 12(7):2685–2705. [PubMed: 1613552]

Harris KM, Weinberg RJ. 2012 Ultrastructure of synapses in the mammalian brain. Cold Spring Harb Perspect Biol 4(5).

Hilgetag CC, Burns GA, O'Neill MA, Scannell JW, Young MP. 2000 Anatomical connectivity defines the organization of clusters of cortical areas in the macaque monkey and the cat. Philosophical transactions of the Royal Society of London Series B, Biological sciences 355(1393):91–110. [PubMed: 10703046]

Hilgetag CC, Medalla M, Beul SF, Barbas H. 2016 The primate connectome in context: Principles of connections of the cortical visual system. Neuroimage 134:685–702. [PubMed: 27083526]

Holtmaat A, Svoboda K. 2009 Experience-dependent structural synaptic plasticity in the mammalian brain. Nat Rev Neurosci 10(9):647–658. [PubMed: 19693029]

Kasthuri N, Hayworth KJ, Berger DR, Schalek RL, Conchello JA, Knowles-Barley S, Lee D, Vazquez-Reina A, Kaynig V, Jones TR, Roberts M, Morgan JL, Tapia JC, Seung HS, Roncal WG, Vogelstein JT, Burns R, Sussman DL, Priebe CE, Pfister H, Lichtman JW. 2015 Saturated Reconstruction of a Volume of Neocortex. Cell 162(3):648–661. [PubMed: 26232230]

Kawaguchi Y, Karube F, Kubota Y. 2006 Dendritic branch typing and spine expression patterns in cortical nonpyramidal cells. Cereb Cortex 16(5):696–711. [PubMed: 16107588]

Larkman AU. 1991 Dendritic morphology of pyramidal neurones of the visual cortex of the rat: III. Spine distributions. J Comp Neurol 306(2):332–343. [PubMed: 1711059]

Li Z, Burrone J, Tyler WJ, Hartman KN, Albeanu DF, Murthy VN. 2005 Synaptic vesicle recycling studied in transgenic mice expressing synaptopHluorin. Proc Natl Acad Sci U S A 102(17):6131–6136. [PubMed: 15837917]

London M, Hausser M. 2005 Dendritic computation. Annual review of neuroscience 28:503–532.

Ludvigson AE, Luebke JI, Lewis J, Peters A. 2011 Structural abnormalities in the cortex of the rTg4510 mouse model of tauopathy: a light and electron microscopy study. Brain Struct Funct 216(1):31–42. [PubMed: 21152933]

Luebke JI, Medalla M, Amatrudo JM, Weaver CM, Crimins JL, Hunt B, Hof PR, Peters A. 2013 Age-Related Changes to Layer 3 Pyramidal Cells in the Rhesus Monkey Visual Cortex. Cereb Cortex.

Markram H, Muller E, Ramaswamy S, Reimann MW, Abdellah M, Sanchez CA, Ailamaki A, Alonso-Nanclares L, Antille N, Arsever S, Kahou GA, Berger TK, Bilgili A, Buncic N, Chalimourda A, Chindemi G, Courcol JD, Delalondre F, Delattre V, Druckmann S, Dumusc R, Dynes J, Eilemann S, Gal E, Gevaert ME, Ghobril JP, Gidon A, Graham JW, Gupta A, Haenel V, Hay E, Heinis T, Hernando JB, Hines M, Kanari L, Keller D, Kenyon J, Khazen G, Kim Y, King JG, Kisvarday Z, Kumbhar P, Lasserre S, Le Be JV, Magalhaes BR, Merchan-Perez A, Meystre J, Morrice BR, Muller J, Munoz-Cespedes A, Muralidhar S, Muthurasa K, Nachbaur D, Newton TH, Nolte M, Ovcharenko A, Palacios J, Pastor L, Perin R, Ranjan R, Riachi I, Rodriguez JR, Riquelme JL, Rossert C, Sfyrakis K, Shi Y, Shillcock JC, Silberberg G, Silva R, Tauheed F, Telefont M, Toledo-Rodriguez M, Trankler T, Van Geit W, Diaz JV, Walker R, Wang Y, Zaninetta SM, DeFelipe J, Hill SL, Segev I, Schurmann F. 2015 Reconstruction and Simulation of Neocortical Microcircuitry. Cell 163(2):456–492. [PubMed: 26451489]

Matsuzaki M, Ellis-Davies GC, Nemoto T, Miyashita Y, Iino M, Kasai H. 2001 Dendritic spine geometry is critical for AMPA receptor expression in hippocampal CA1 pyramidal neurons. Nature neuroscience 4(11):1086–1092. [PubMed: 11687814]

McGuire BA, Gilbert CD, Rivlin PK, Wiesel TN. 1991 Targets of horizontal connections in macaque primary visual cortex. J Comp Neurol 305(3):370–392. [PubMed: 1709953]

Medalla M, Barbas H. 2009 Synapses with inhibitory neurons differentiate anterior cingulate from dorsolateral prefrontal pathways associated with cognitive control. Neuron 61(4):609–620. [PubMed: 19249280]

Medalla M, Barbas H. 2010 Anterior cingulate synapses in prefrontal areas 10 and 46 suggest differential influence in cognitive control. J Neurosci 30(48):16068–16081. [PubMed: 21123554]

Medalla M, Lera P, Feinberg M, Barbas H. 2007 Specificity in inhibitory systems associated with prefrontal pathways to temporal cortex in primates. Cereb Cortex 17 Suppl 1:i136–150. [PubMed: 17725996]

Medalla M, Luebke JI. 2015 Diversity of glutamatergic synaptic strength in lateral prefrontal versus primary visual cortices in the rhesus monkey. J Neurosci 35(1):112–127. [PubMed: 25568107]

Melchitzky DS, Sesack SR, Pucak ML, Lewis DA. 1998 Synaptic targets of pyramidal neurons providing intrinsic horizontal connections in monkey prefrontal cortex. J Comp Neurol 390(2): 211–224. [PubMed: 9453665]

Meyer D, Bonhoeffer T, Scheuss V. 2014 Balance and stability of synaptic structures during synaptic plasticity. Neuron 82(2):430–443. [PubMed: 24742464]

Murthy VN, Schikorski T, Stevens CF, Zhu Y. 2001 Inactivity produces increases in neurotransmitter release and synapse size. Neuron 32(4):673–682. [PubMed: 11719207]

Murthy VN, Sejnowski TJ, Stevens CF. 1997 Heterogeneous release properties of visualized individual hippocampal synapses. Neuron 18(4):599–612. [PubMed: 9136769]

Nimchinsky EA, Sabatini BL, Svoboda K. 2002 Structure and function of dendritic spines. Annu Rev Physiol 64:313–353. [PubMed: 11826272]

Nusser Z, Lujan R, Laube G, Roberts JD, Molnar E, Somogyi P. 1998 Cell type and pathway dependence of synaptic AMPA receptor number and variability in the hippocampus. Neuron 21(3): 545–559. [PubMed: 9768841]

Nys J, Scheyltjens I, Arckens L. 2015 Visual system plasticity in mammals: the story of monocular enucleation-induced vision loss. Front Syst Neurosci 9:60. [PubMed: 25972788]

O'Kusky J, Colonnier M. 1982 A laminar analysis of the number of neurons, glia, and synapses in the adult cortex (area 17) of adult macaque monkeys. J Comp Neurol 210(3):278–290. [PubMed: 7142443]

Olshausen BA, Field DJ. 2004 Sparse coding of sensory inputs. Curr Opin Neurobiol 14(4):481–487. [PubMed: 15321069]

Pandya DN, Seltzer B, Petrides M, Cipolloni PB. 2015 Cerebral Cortex: Architecture, Connections, and the Dual Origin Concept. New York, NY: Oxford University Press.

Panzeri S, Brunel N, Logothetis NK, Kayser C. 2010 Sensory neural codes using multiplexed temporal scales. Trends in neurosciences 33(3):111–120. [PubMed: 20045201]

Perrin S 2014 Preclinical research: Make mouse studies work. Nature 507(7493):423–425. [PubMed: 24678540]

Peters A, Palay SL, Webster HD. 1991 The Fine Structure of the Nervous System. New York: Oxford University Press.

Peters A, Sethares C. 1991 Organization of pyramidal neurons in area 17 of monkey visual cortex. J Comp Neurol 306(1):1–23. [PubMed: 1710236]

Peters A, Sethares C, Luebke JI. 2008 Synapses are lost during aging in the primate prefrontal cortex. Neuroscience 152(4):970–981. [PubMed: 18329176]

Petrides M, Tomaiuolo F, Yeterian EH, Pandya DN. 2012 The prefrontal cortex: comparative architectonic organization in the human and the macaque monkey brains. Cortex 48(1):46–57. [PubMed: 21872854]

Raghavachari S, Lisman JE. 2004 Properties of quantal transmission at CA1 synapses. Journal of neurophysiology 92(4):2456–2467. [PubMed: 15115789]

Rakic P 2002 Neurogenesis in adult primate neocortex: an evaluation of the evidence. Nat Rev Neurosci 3(1):65–71. [PubMed: 11823806]

Rakic P 2009 Evolution of the neocortex: a perspective from developmental biology. Nat Rev Neurosci 10(10):724–735. [PubMed: 19763105]

Rall W 1962 Theory of physiological properties of dendrites. Annals of the New York Academy of Sciences 96:1071–1092. [PubMed: 14490041]

Rall W 1964 Theoretical significance of dendritic trees for neuronal input-output relations In: Reiss RF, ed. Neural Theory and Modeling. Palo Alto, CA: Stanford University Press p 73–97.

Ramón y Cajal S 1894 Estructura intima de los centros nerviosos. Rev Ciencias Med 20:145–160.

Ramón y Cajal S 1995 Histology of the nervous system of man and vertebrates. Swanson NSLW, ed. Oxford, NY: Oxford Universiy Press.

Rollenhagen A, Klook K, Satzler K, Qi G, Anstotz M, Feldmeyer D, Lubke JH. 2015 Structural determinants underlying the high efficacy of synaptic transmission and plasticity at synaptic boutons in layer 4 of the adult rat 'barrel cortex'. Brain Struct Funct 220(6):3185–3209. [PubMed: 25084745]

Rollenhagen A, Lubke JH. 2006 The morphology of excitatory central synapses: from structure to function. Cell Tissue Res 326(2):221–237. [PubMed: 16932936]

Sabatini BL, Oertner TG, Svoboda K. 2002 The life cycle of Ca(2+) ions in dendritic spines. Neuron 33(3):439–452. [PubMed: 11832230]

Schikorski T, Stevens CF. 2001 Morphological correlates of functionally defined synaptic vesicle populations. Nature neuroscience 4(4):391–395. [PubMed: 11276229]

Schuz A, Palm G. 1989 Density of neurons and synapses in the cerebral cortex of the mouse. J Comp Neurol 286(4):442–455. [PubMed: 2778101]

Sjostrom PJ, Rancz EA, Roth A, Hausser M. 2008 Dendritic excitability and synaptic plasticity. Physiological reviews 88(2):769–840. [PubMed: 18391179]

Spacek J, Harris KM. 1997 Three-dimensional organization of smooth endoplasmic reticulum in hippocampal CA1 dendrites and dendritic spines of the immature and mature rat. J Neurosci 17(1): 190–203. [PubMed: 8987748]

Spruston N 2008 Pyramidal neurons: dendritic structure and synaptic integration. Nat Rev Neurosci 9(3):206–221. [PubMed: 18270515]

Takumi Y, Ramirez-Leon V, Laake P, Rinvik E, Ottersen OP. 1999 Different modes of expression of AMPA and NMDA receptors in hippocampal synapses. Nature neuroscience 2(7):618–624. [PubMed: 10409387]

Testa-Silva G, Verhoog MB, Linaro D, de Kock CP, Baayen JC, Meredith RM, De Zeeuw CI, Giugliano M, Mansvelder HD. 2014 High bandwidth synaptic communication and frequency tracking in human neocortex. PLoS Biol 12(11):e1002007. [PubMed: 25422947]

Timbie C, Barbas H. 2014 Specialized pathways from the primate amygdala to posterior orbitofrontal cortex. J Neurosci 34(24):8106–8118. [PubMed: 24920616]

Tong G, Jahr CE. 1994 Multivesicular release from excitatory synapses of cultured hippocampal neurons. Neuron 12(1):51–59. [PubMed: 7507341]

Tropea D, Van Wart A, Sur M. 2009 Molecular mechanisms of experience-dependent plasticity in visual cortex. Philosophical transactions of the Royal Society of London Series B, Biological sciences 364(1515):341–355. [PubMed: 18977729]

Verhoog MB, Goriounova NA, Obermayer J, Stroeder J, Hjorth JJ, Testa-Silva G, Baayen JC, de Kock CP, Meredith RM, Mansvelder HD. 2013 Mechanisms underlying the rules for associative plasticity at adult human neocortical synapses. J Neurosci 33(43):17197–17208. [PubMed: 24155324]

Vogels TP, Rajan K, Abbott LF. 2005 Neural network dynamics. Annual review of neuroscience 28:357–376.

Zikopoulos B, Barbas H. 2007 Parallel driving and modulatory pathways link the prefrontal cortex and thalamus. PLoS One 2(9):e848. [PubMed: 17786219]

Zilles K, Palomero-Gallagher N, Schleicher A. 2004 Transmitter receptors and functional anatomy of the cerebral cortex. J Anat 205(6):417–432. [PubMed: 15610391]

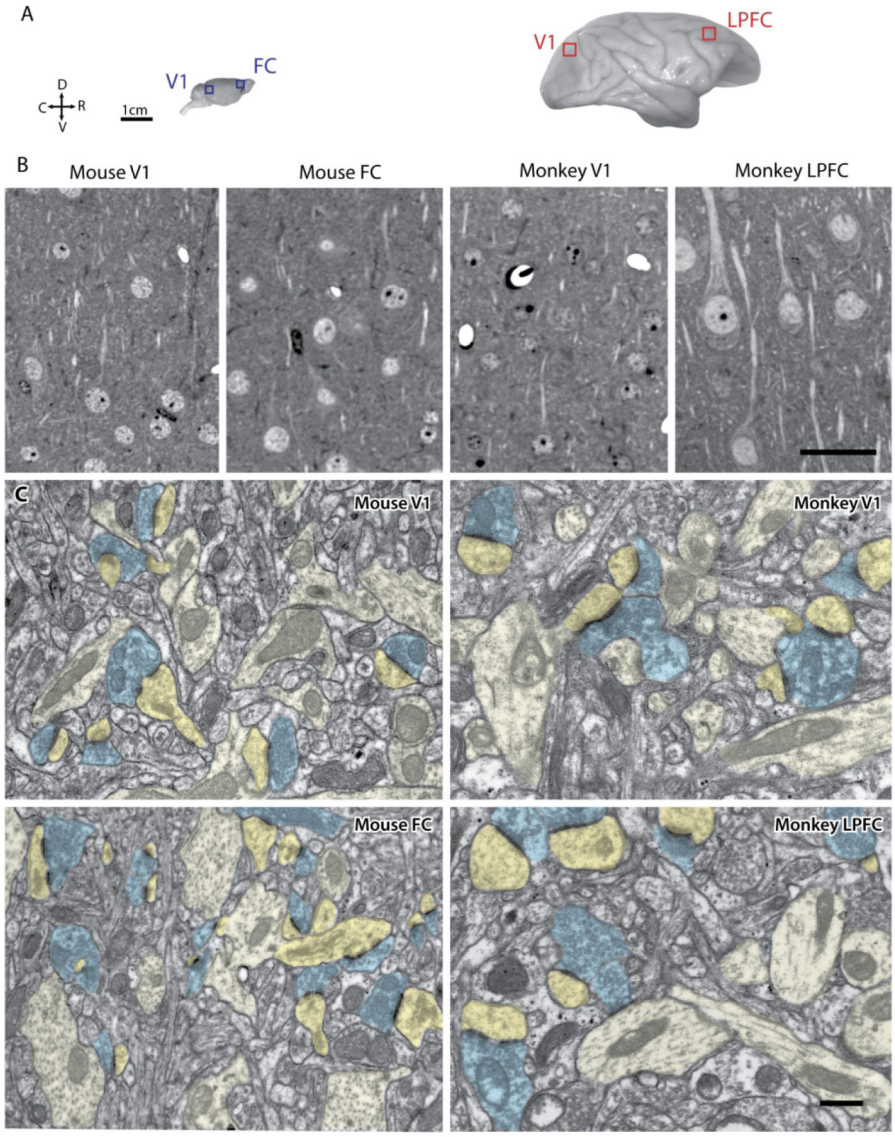

Figure 1.

Cytoarchitecture and ultrastructure of visual and frontal cortices in mouse and rhesus monkey. A) Lateral views of the mouse brain showing sampling sites in V1 and FC, and of the rhesus monkey brain showing sampling sites in V1 and LPFC, where tissue blocks for EM were taken. Axes: R, rostral; C, caudal; D, dorsal; V, ventral. B) Photomicrographs of semi-thick (1 μm) coronal sections stained with Toluidine blue showing distribution of neuronal somata and neuropil in mouse and monkey visual and frontal cortices. C) Electron micrographs in L2-3 of mouse V1, mouse FC, monkey V1 and monkey, showing axonal boutons (blue) forming asymmetric synapses targeting spines (dark yellow) and dendrites (light yellow). Scale bars: A = 1 cm, B = 50 μm, C = 0.5 μm.

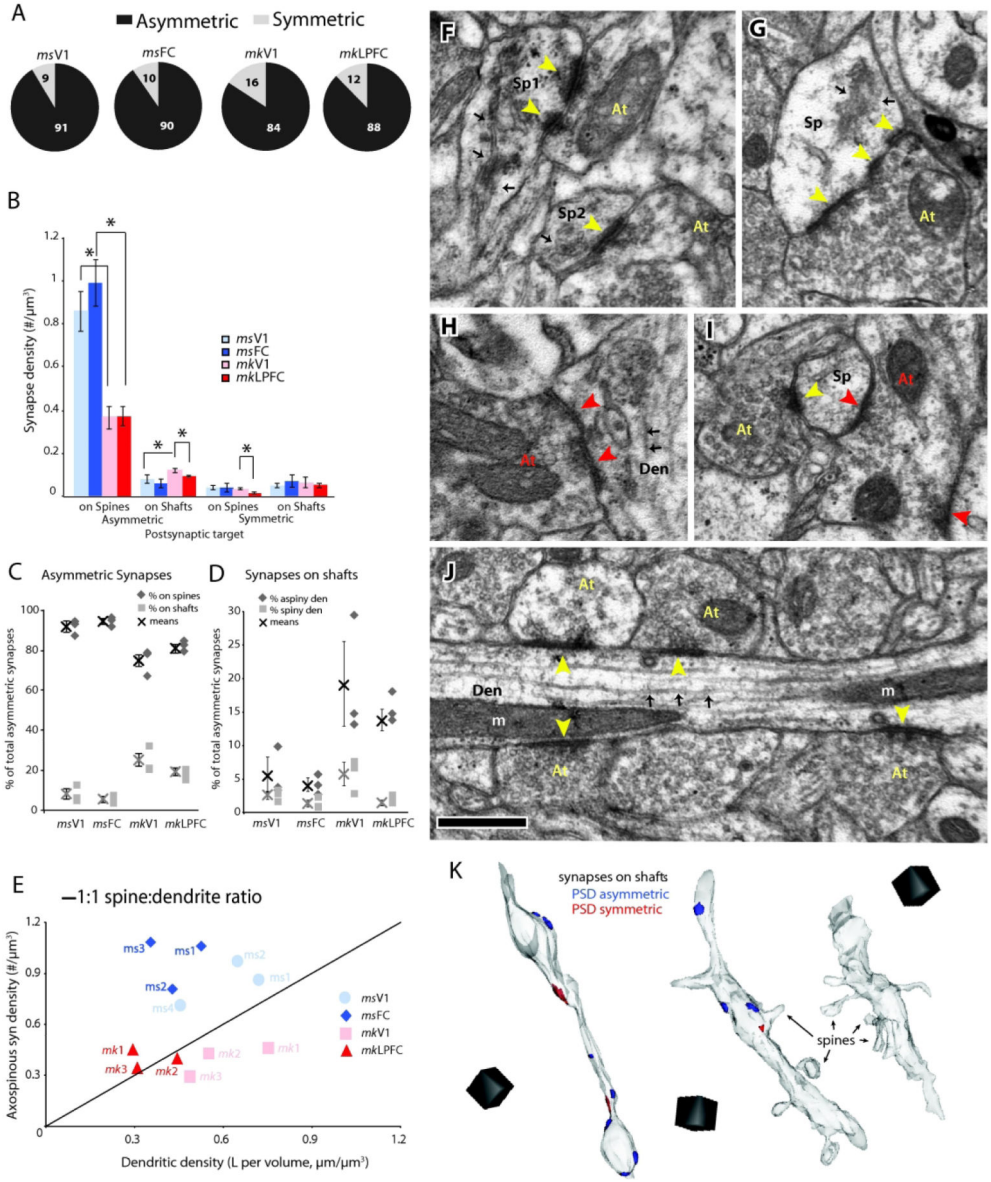

Figure 2.

Density and distribution of synapses in L2-3 neuropil of visual and frontal cortices of mouse versus monkey. A) Relative proportions of asymmetric (black) and symmetric (light gray) synapses. B) Numerical density of asymmetric and symmetric axospinous and shaft synapses. *$p < 0.01$; C) Relative proportion of asymmetric axospinous (black) and shaft (light gray) synapses. D) Relative proportion of asymmetric shaft synapses on aspiny (black) versus spiny (light gray) dendrites. E) Relationship between axospinous synaptic density and total length of spiny dendrites in the L2-3 neuropil of each individual mouse and monkey. F-J) Electron micrographs of different types of synapses with their PSD (arrowheads), presynaptic axon terminal (At) and postsynaptic spine (Sp) or dendrite (Den): F) Two axospinous asymmetric synapses (yellow arrowheads) formed on spines with SA/SER (black arrows) in mouse FC; the synapse on Sp1 is perforated and on Sp2 is non-perforated. G) Perforated asymmetric synapse formed on spine with SA/SER in monkey LPFC. H)

Symmetric shaft synapse (red arrowheads) targeting the dendritic shaft (Den) in mouse V1. Note the presence of microtubules (black arrows) in the dendrite. I) Two synapses on a single spine (Sp) in monkey V1, one is asymmetric (yellow arrowhead) and one is symmetric (red arrowhead) whose axon terminal forms another symmetric synapse on another nearby spine. J) An aspiny/smooth dendrite from monkey LPFC receiving a row of asymmetric shaft synapses (yellow arrowheads) -- a characteristic morphology of an inhibitory neuron. K) 3D reconstructions showing examples of dendrites: an aspiny dendrite (left) with no visible spines and a high density of asymmetric synapses on the shaft from monkey LFC; a sparsely spiny dendrite (middle) with low asymmetric axospinous but high shaft synapse density from monkey V1; and a spiny dendrite (right), with high asymmetric axospinous synapse density but no (or low number of) asymmetric shaft synapses, from mouse FC. Scale: F-J, 0.5 μm, K = $(1\ \mu m)^3$

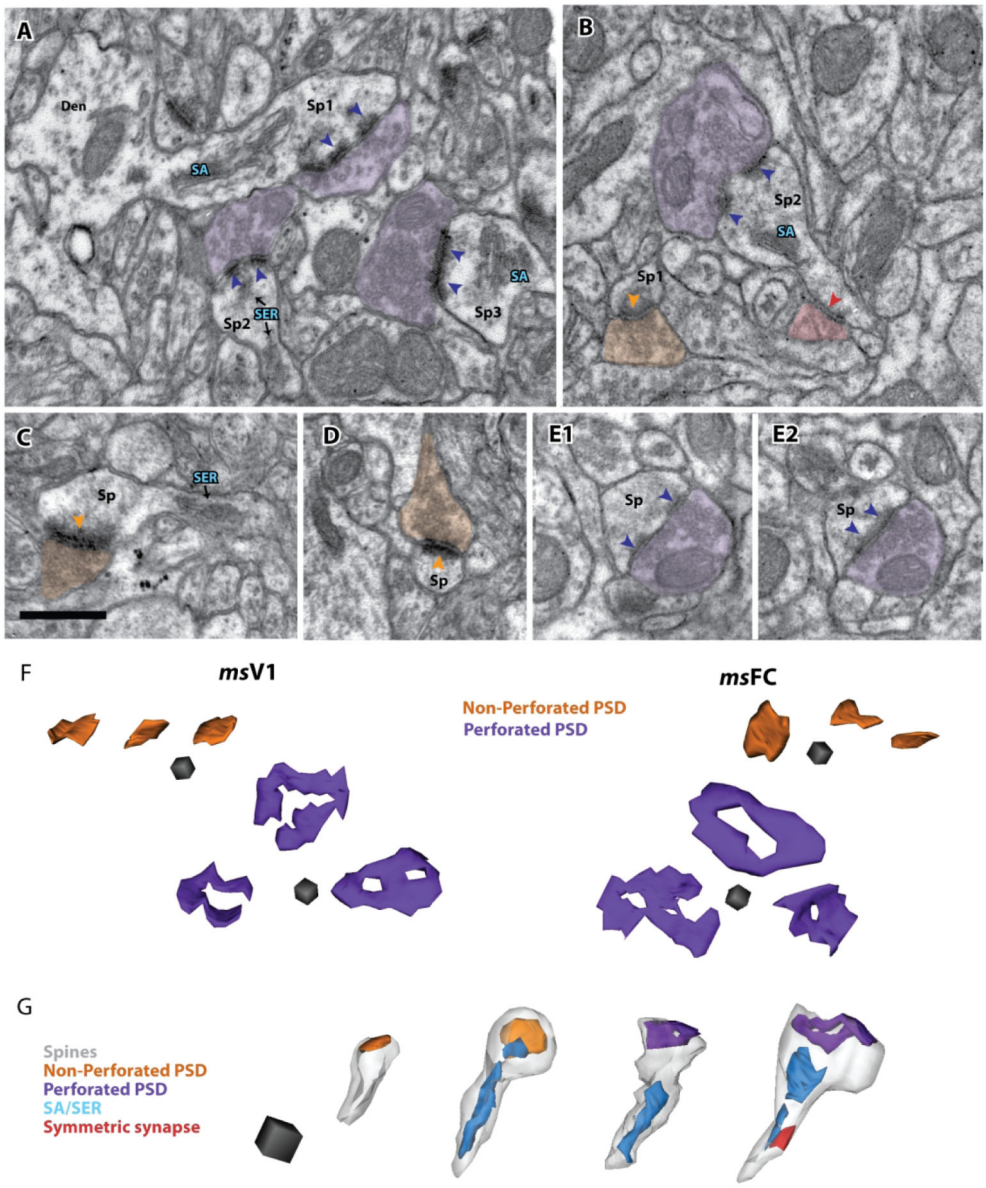

Figure 3.

Electron micrographs and 3D reconstructions of axospinous asymmetric synapses in the L2-3 neuropil of mouse FC and V1. A-E) Electron micrographs showing distinct ultrastructural types of asymmetric axospinous synapses – receiving perforated (purple) versus non-perforated (orange) synapses and containing spine apparatus (SA) or smooth endoplasmic reticulum (SER, blue): A) Examples of 3 spines receiving perforated synapses (purple arrowheads) and containing SA (Sp1 and Sp3) or SER (Sp2) in mouse FC. One spine (Sp1) is seen emanating from parent dendrite (Den). Spine 3 appears not to be perforated in the current section but perforation is visible in adjacent serial sections (not shown). B) Two spines in mouse V1, one (Sp1) receives a non-perforated synapse (orange arrowheads) and has no SA/SER, another (Sp2) receives a perforated synapse (purple) and contains an SA/SER. C, D) Two examples of spines forming non perforated synapses, on

mouse FC, one contains SER in its neck (C) and the other does not contain any SA/SER (D). E1, E2) Adjacent serial images showing a spine receiving a perforated synapse and containing no SA/SER. F) 3D reconstructions top flat surface view of non-perforated and perforated axospinous synapses in mouse V1 and FC. G) 3D reconstructions of spines (left to right): with non-perforated synapse and no SA/SER; with non-perforated synapse and with SA/SER in its head and neck; with perforated synapse and with SA/SER only in its neck; and with perforated synapse and with SA/SER in its head and neck. Scale bars: A-E = 0.5 μm, F = $(0.1\ \mu m)^3$, G = $(0.25\ \mu m)^3$

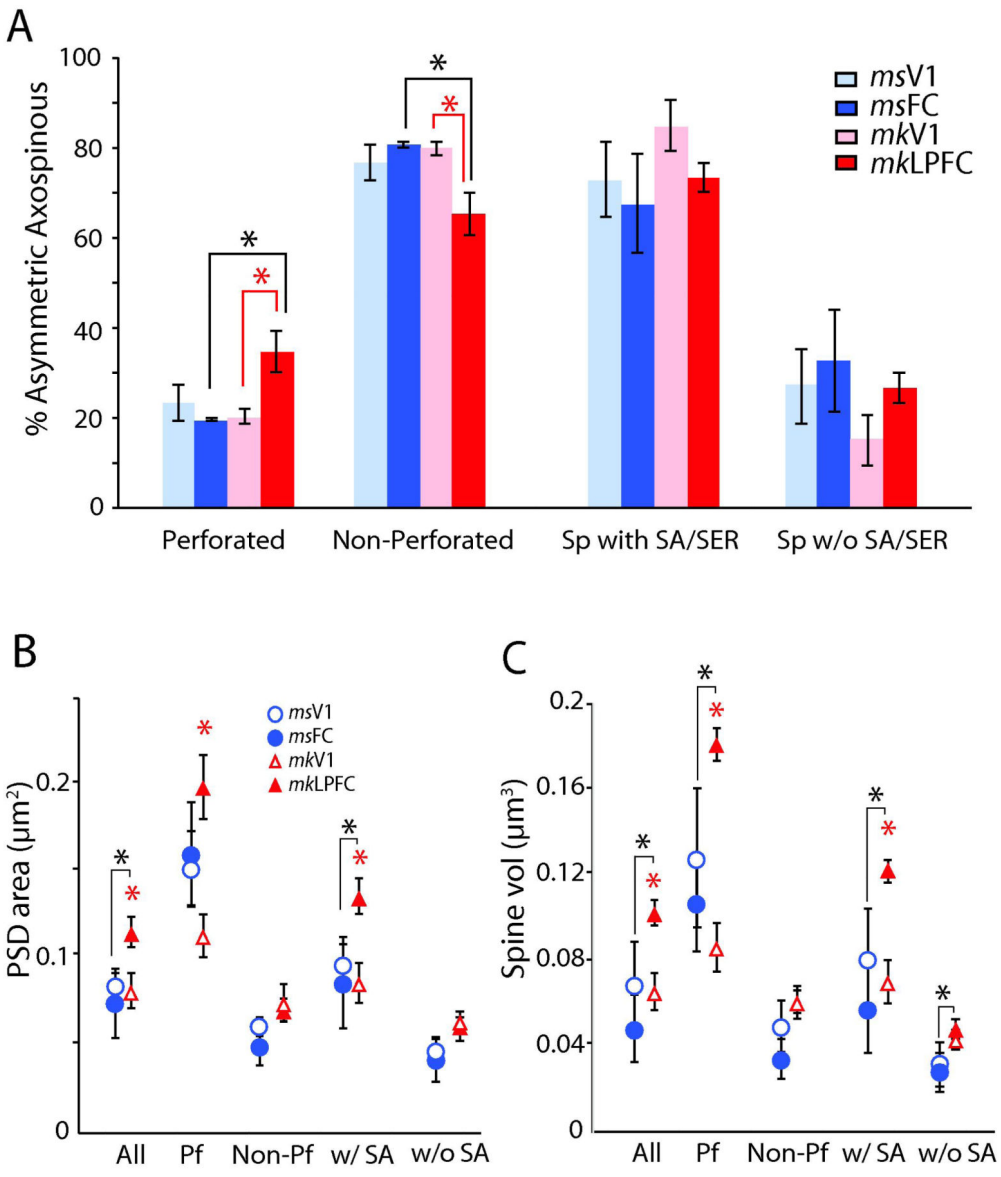

Figure 4.

Proportion and size of distinct types of asymmetric axospinous synapses and spines in L2-3 neuropil of visual and frontal cortices of mouse versus monkey. A) Proportion of asymmetric axospinous synapses with or without perforations, or associated with spines with or without SA/SER. *p < 0.05, monkey LPFC versus V1 (red asterisk), and mouse versus monkey (black asterisk). B) Mean PSD surface area and; C) mean spine volume for each type of asymmetric axospinous synapse. *p < 0.05 monkey LPFC versus V1 (red asterisk), and mouse FC versus monkey LPFC (black asterisk).

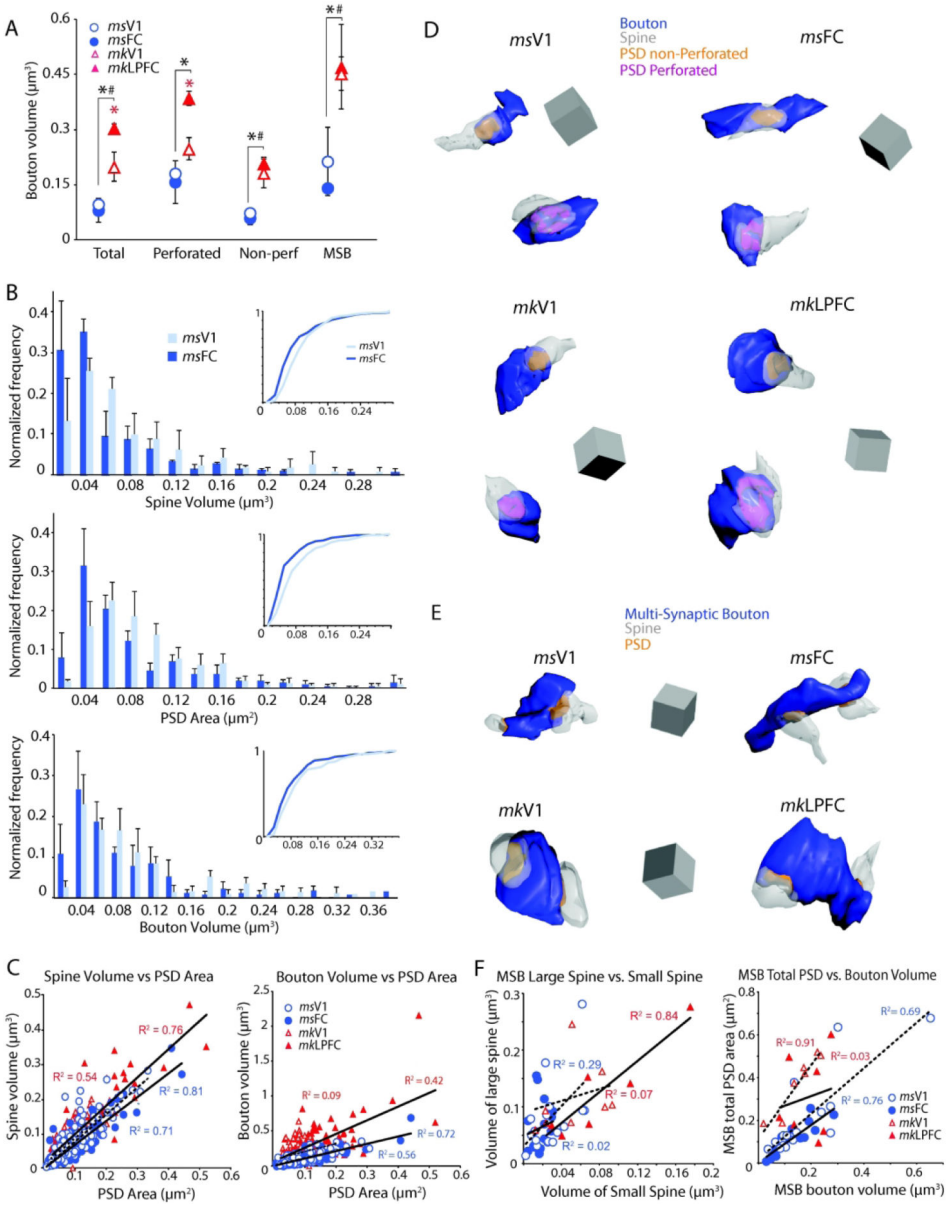

Figure 5.

Relationships between pre- and post-synaptic components of asymmetric axospinous synapses in L2-3 neuropil of visual and frontal cortices of mouse versus monkey. A) Mean volume of total presynaptic axonal boutons and sub-populations associated with perforated PSDs, non-perforated PSDs, and more than one postsynaptic spine (n=16 for mouse V1 and FC, n=7 for monkey V1 and LPFC). *p< 0.01 monkey LPFC versus V1 (red asterisk); *p < 0.01 mouse FC versus monkey LPFC (black asterisk); #p < 0.05 mouse V1 versus monkey V1. B) Histograms demonstrating the normalized frequency of spine volumes, PSD areas and volumes of single-synaptic boutons in mouse V1 versus FC neuropil. C) Scatter plots demonstrating relationships between spine volume and PSD area (left) and PSD area and volume of bouton forming a single axospinous synapse (right). D) 3D reconstructions of boutons each forming a single asymmetric synapse with one spine; and E) of multi-synaptic

boutons (MSBs) forming synapses on multiple spines in mouse V1, mouse FC, monkey V1 and monkey LPFC. Scale = $(0.5\ \mu m)^3$. F) Scatter plots demonstrating relationships between the volume of the larger versus smaller spine targeted by each MSB (left) and between the total PSD area versus bouton volume of each MSB (right).

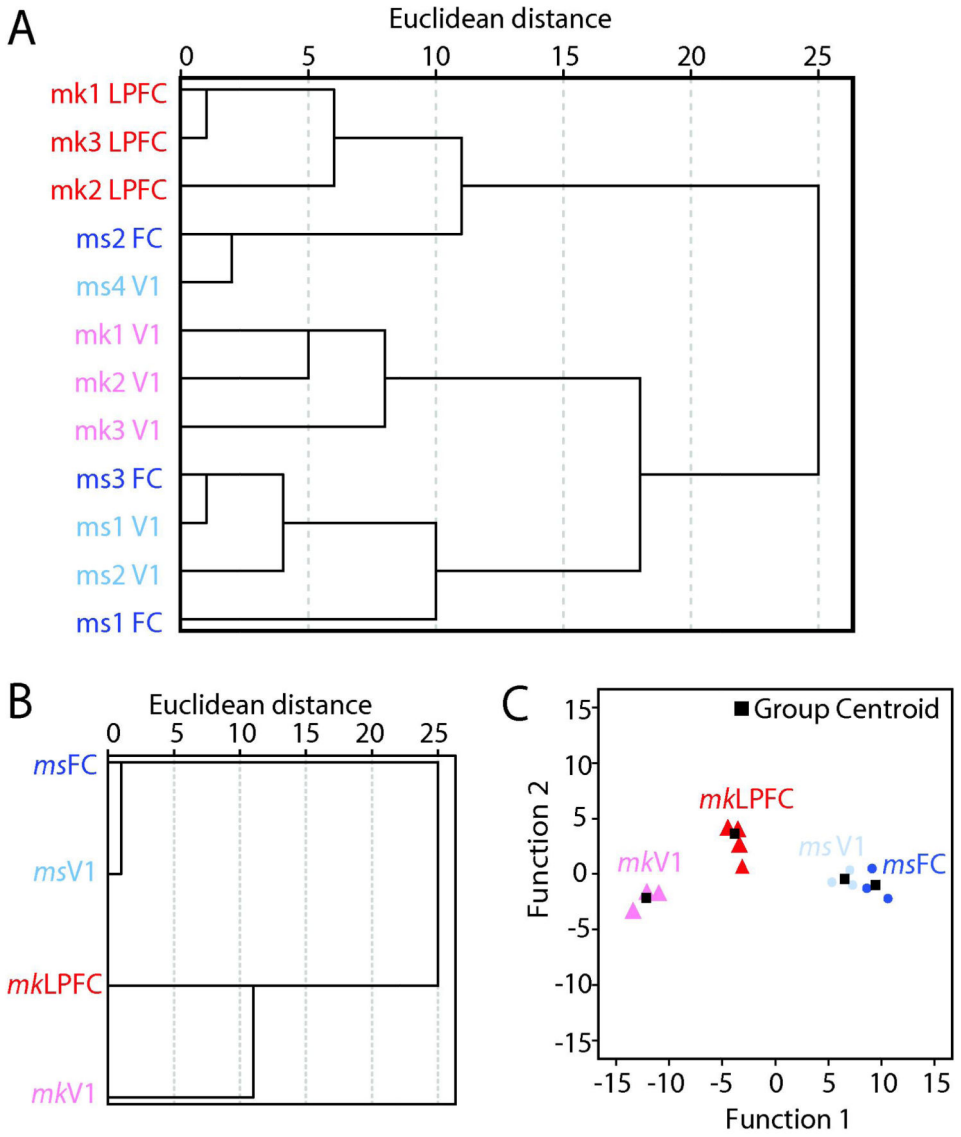

Figure 6.

Relative similarity and classification of asymmetric synapses in L2-3 neuropil of mouse and rhesus monkey frontal and visual cortices. A) Hierarchical cluster tree showing the relative (dis)similarities for individual subjects in each of the four groups, based on all ultrastructural variables combined for each subject. B) Hierarchical cluster and discriminant analyses showing the relative (dis)similarities, based on all mean ultrastructural variables combined for each of the four groups. C) Discriminant analysis plot showing clustering of individual cells (discriminant functions: df_1, eigenvalue = 110.45, r = 0.996, Wilks' $\lambda < 0.001$, p = 0.014; df_2 eigenvalue = 7.26, r = 0.937, Wilks' $\lambda = 0.027$, p = 0.203; df_3 eigenvalue = 3.53, r = 0.883, Wilks' $\lambda = 0.221$, p = 0.273).